

Design Approaches and Electromechanical Modeling of Conformable Piezoelectric-Based Ultrasound Systems

Nikta Amiri, Aastha Shah, Amit Kumar Bhayadia, Chia-Chen Yu, M. Amin Karami, and Canan Dagdeviren*

Painless, needleless delivery of drugs through the skin can be realized through a phenomenon called sonophoresis by applying an ultrasound field to the biological tissue. Development of wearable embodiments of such systems demands comprehensive characterization of both the physical mechanism of sonophoresis as well as wearability parameters. Here, we present a framework for analyzing disk-type piezoelectric transducers in a polymeric substrate to create acoustic cavitation in a fluid coupling medium for sonophoresis applications. The device design and operating parameters such as the working frequency, applied voltage range, acoustic pressure distribution, and transducer spacing were determined using a finite element method (FEM), and verified with experimental measurements. The influence of the surrounding water and tank reflections on the acoustic pressure field, and the interaction between the elements in the array structure were also studied. Finally, the impact of skin and the substrate geometry on the acoustic pressure fields was characterized to simulate the *in vivo* use-case of the system. These analytical models can be used to guide critical parameters for device design such as the separation distance of the piezoelectric transducer from the skin boundary. We envision that this tool box will support rapid design iteration for realization of wearable ultrasound systems.

1. Introduction

Increased consumer interest in healthy-looking skin has provided great impetus for research in transdermal drug

N. Amiri, A. K. Bhayadia, M. A. Karami
Department of Mechanical and Aerospace Engineering
University at Buffalo
Buffalo, NY 14260, USA

A. Shah, C.-C. Yu, C. Dagdeviren
Media Lab
Massachusetts Institute of Technology
Cambridge, MA 02139, USA
E-mail: canand@media.mit.edu

C.-C. Yu
Department of Electrical Engineering and Computer Science
Massachusetts Institute of Technology
Cambridge, MA 02139, USA

 The ORCID identification number(s) for the author(s) of this article can be found under <https://doi.org/10.1002/adrs.202300175>

© 2024 The Authors. Advanced Sensor Research published by Wiley-VCH GmbH. This is an open access article under the terms of the [Creative Commons Attribution](#) License, which permits use, distribution and reproduction in any medium, provided the original work is properly cited.

DOI: 10.1002/adrs.202300175

delivery systems in recent years, owing to its non-invasiveness, programmable dose rate, and convenience.^[1] A number of methods have been explored to achieve percutaneous transport of drugs and cosmetics, including passive diffusion patches^[2] mechanical,^[3] chemical^[4] or mechano-chemical enhancers,^[5] application of electric fields to the skin employing iontophoresis,^[6] electroporation^[7] and sonophoresis^[8] or combined strategies involving two or more of the above,^[9,10] Prausnitz's comprehensive review papers provide a comparison on the various approaches mentioned above,^[11,12] Prominent among these is sonophoresis, the application of ultrasound energy to instantiate acoustic cavitation *in situ*, within or on the skin surface, and disrupt the tightly packed lipid-bilayer structure of the stratum corneum to enhance the transport of drugs.

However, acoustic cavitation is a highly sensitive stochastic phenomenon, where

multiple systems as well as environmental parameters such as transducer properties, spatial geometry^[13] and choice of coupling medium,^[14] dissolved gas content,^[15] and heterogeneity and separation of target membrane^[16] profoundly impact each instance of cavitation. Controlling the cavitation dynamics to achieve repeatable performance *in vivo* demands rigorous characterization of the working physics of sonophoresis. Multiphysics FEM simulations are valuable tools in understanding the acoustic behavior of the fluid medium where experimental methods encounter practical limits in obtaining measurements, for example, in close vicinity of the ultrasound transducer where the electromagnetic coupling between the transducer and the hydrophone can confound the small signal pick-up of the pressure field. A number of studies have provided well-developed theoretical and FEM models for studying the electrostatic-acoustic behavior of ultrasound transducers for various applications – including electrical impedance profiles for high-intensity focused ultrasound (HIFU) transducers in heat therapy,^[17] vibrational modal analysis for disk transducer in a fluid medium,^[18] reduced-order modeling of pressure fields for ultrasound power transfer *in vitro*,^[19,20] and cavitation threshold characterization for a horn-type ultrasound sono-reactor.^[21] Each of the above works provides a comprehensive discussion on one important aspect of the modeling of the ultrasound transducer or pressure regime. Specifically, Martinez's

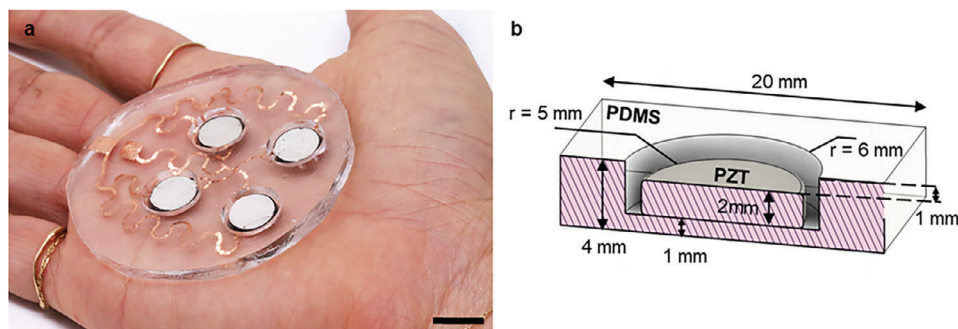


Figure 1. Conformable ultrasound patch for cavitation-enhanced transdermal drug delivery. a) Photograph of device with a 2×2 array of piezoelectric actuators in a PDMS substrate. Scale bar 1 cm. b) Geometrical detail of a single piezoelectric actuator in PDMS cavity.

paper on HIFU^[17] provides an experimentally-validated approach for characterizing the electric impedance behavior of disc-type transducers. Bhargava's work^[19] presents a penetrating commentary on the impact of nonlinearities in acoustic wave propagation and material parameters on ultrasound delivery, which is an important consideration when designing devices for inherently nonlinear systems, such as human tissue. Wei^[21] demonstrates theoretical and experimental methods for generating acoustic pressure maps for the determination of cavitation-prone zones in a finite fluid volume around the transducer. All of the above individually are critical considerations in the development of ultrasound devices, yet there is no literature that presents a full developmental pipeline of modeling and characterization milestones that must be met to create integrated ultrasound systems. Primarily, as we move toward more applied and wearable embodiments of these ultrasound technologies,^[22,23] it is important to determine an optimized pipeline for rapid electrostatic and mechano-acoustic characterization of piezoelectric transducers, and the impact of soft encapsulants and human tissue on their performance in vivo as well.

In this study, we propose the development of a conformable, wearable platform of piezoelectric disk-type transducers (PZT-Ds) embedded in a soft polymeric substrate with patterned cavities for delivering low-frequency sonophoresis (LFS) to the skin within a contained fluid pocket (**Figure 1a**). Conformable wearable platforms provide unique opportunities to interface electronics with soft, curvilinear body targets for both physiological sensing and actuation,^[24,25] Using biocompatible polymeric materials with mechanical properties that closely match those of living tissue,^[26] we can create personalized designs for intimate contact with the skin surface.^[27] Computational and theoretical models for the same can greatly contribute to the success of these designs in vivo,^[28,29] In this device, the polydimethylsiloxane (PDMS) substrate is used to create geometrical features to act as the drug reservoir, and allow controlled positioning of the PZT-D relative to the skin. This report provides a complete pipeline of FEM models for the development of flexible, wearable sonophoresis systems for achieving transdermal drug delivery through the skin. First, we discuss the electromechanical characterization of disk-type transducers including the impedance profiles, vibrational displacements, and mode shapes of PZT-Ds in air and water. Next, the impact of changing geometrical parameters such as the radius and thickness of the PZT-D, and the ad-

dition of polymeric backing and encapsulation on the vibrational behavior of the transducer is examined. The time-varying acoustic pressure fields created by the transducer in water are then characterized using coupled electrostatic and acoustic theoretical models. Far-field pressure values are validated using experimental measurements in the frequency domain, and near-field pressure maps are generated to determine the spatial regions of interest for cavitation nucleation. Finally, 3D FEM models are created for the complete system of a multi-element array of PZT-Ds on a soft substrate, and its interaction with skin.

These studies capture the full spectrum of electro-acoustic and mechano-acoustic models needed to develop LFS systems, where consequently the material properties and design parameters can be rapidly iterated to generate optimized configurations of PZT-D arrays for programmable and large-area delivery of drugs across the human body. We believe this report lays valuable groundwork for the future development of wearable piezoelectric systems and provides a toolbox to aid material scientists and engineers working to realize scalable, sustainable deployment of transdermal drug delivery systems in the consumer industry.

2. Results and Discussion

A Finite Element Analysis (FEA) model is created in COMSOL Multiphysics to simulate the different vibrational modes of the piezoelectric transducer and to perform acoustic pressure analysis for sonophoresis. Details of the physics interface, boundary conditions, geometry, and materials used in the FEA simulations are provided in (Section S1, Supporting Information).

2.1. Electromechanical Characterization of the Piezoelectric Disk (PZT-D) in a Flexible Substrate

2.1.1. Impact of Geometric Parameters on the Resonant Frequency and Displacement

Understanding the electrical impedance response of the PZT-D is fundamental to providing insight into the electrical behavior for a wide range of frequencies. The impedance magnitude depends on the structural and material properties and is a useful way to obtain vibration mode characterization since the electromechanical coupling factor and quality factor can be calculated

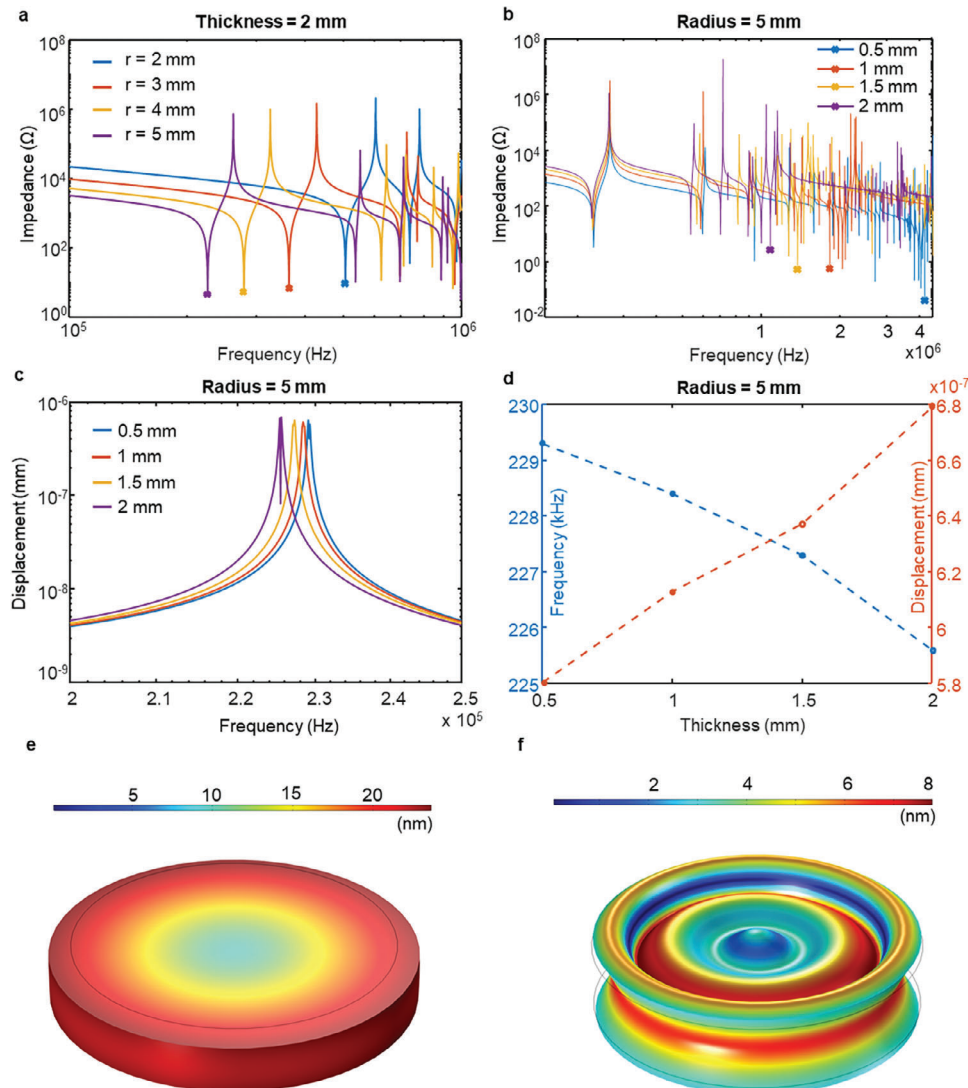


Figure 2. Impact of geometrical parameters on impedance and displacement spectrum of PZT-D. a) Impedance profile for various PZT-D radii for a fixed thickness of 2 mm. b) Impedance profile for various PZT-D thicknesses for a fixed radius of 5 mm. The “x”s mark the thickness resonance frequencies corresponding to the minimum impedance. c) Peak displacement of PZT-D element (at the center of the face) for different PZT-D thickness at a fixed radius of 5 mm. d) Shift in peak placement and resonance frequency for different PZT-D thickness for a fixed radius of 5 mm. The shift in resonance frequency is calculated for discrete values (solid dots), and the trend is extrapolated using the dashed lines. Mode shapes showing peak displacements in nm for e) radial (220 kHz) and f) thickness mode (1 MHz) of vibration for a PZT-D ($r = 5$ mm, $t = 2$ mm).

from the impedance curve. The occurrence of natural frequencies of the piezoelectric transducer including both resonances (local minimums) and antiresonances (local maximums) can also be found via the impedance frequency spectrum.

The impedance from FEM simulations is calculated based on the ratio between voltage and current for the electrodes over the frequency range of interest. The total electric current flowing through the transducer is obtained by differentiating the charge density (Q) with respect to time (t) and integrating it over the electrode area. Electric charge is expressed in the exponential form of $Q = Q_0 e^{i\omega t}$ which yields the current magnitude of $|I| = |\partial Q / \partial t| = \omega_0 Q = \int D_3 dA$, where D_3 is the electric displacement in z direction and A is the surface area.^[30] The impedance magnitude is then calculated by the general ohm law as $|Z| = |V| / |I|$.

Figure 2a,b shows the impedance spectra of the piezoelectric transducers with different dimensions obtained by the FEM analysis.

The radius of the piezoelectric transducer is varied (2, 3, 4, and 5 mm) while keeping the thickness constant at 2 mm to explore the effect of radial dimension on the impedance frequency spectrum. The lowest radial resonant frequency of 220 kHz is observed for the PZT-D with a radius of 5 mm. It is observed that increasing the radius of the piezo shifts the resonant frequency down from 550 kHz at 2 mm to 220 kHz at 5 mm as shown in Figure 2a. However, the change in radius has a negligible impact on the resonant frequency of the thickness mode close to 1 MHz. Next, the radius is kept constant at 5 mm, and the thickness is varied between 0.5 and 2 mm. This significantly impacts the

resonant frequency of the thickness mode (1.08 MHz at 2 mm to 4.18 MHz at 0.5 mm, marked with “-x” in Figure 2b). This is in accordance with the inverse relationship expected between the resonance frequency and thickness of the crystal. It is also to be noted that the resonance frequency at the radial mode (≈ 220 kHz) remains relatively unchanged for thickness changes (5% variation between the minimum and maximum values, measured with respect to the minimum, 225 kHz). This demonstrates a strong decoupling between the thickness and radial modes of operation of the PZT-Ds, and can be strategically exploited in the design of the patch. For example, the radial mode can be selected as the operating mode of the device, and the thickness can be reduced significantly to achieve a more compact form factor without significantly shifting the resonant frequency and peak displacement attainable at that frequency (Figure 2d). This is desirable from an operational point of view, as the cavitation threshold in a given medium depends strongly on the frequency of the ultrasound energy being applied.

For the PZT-D of interest, ($r = 5$ mm, $t = 2$ mm), we obtain 5 distinct modes in the range of 200 kHz–1.1 MHz. The displacements are in the order of picometers for a $10 V_{pp}$ sweep across the frequency band. Of the 5 modes, the PZT-D exhibits two dominant different types of deformations: radial and thickness. The radial mode involves expansions and contractions along the radius. The through-thickness deformations are swellings in the thickness direction. The relative contributions of the radial and thickness deformation to the total displacement are discussed in (Section S3, Supporting Information). We aim to numerically investigate the vibration characteristics and mode shape for both modes (radial and thickness modes). The free boundary conditions are applied to our FEM model. The relation between the voltage and displacement can be expressed as $-\rho\omega^2u = \nabla \cdot S$, $S = c:\epsilon - e^T E$, where ρ , ω , u , S , c , e , and E are the density, frequency, displacement vector, strain, elasticity, coupling matrix, and electric field vector, respectively. The mode shapes and peak total displacements of the top surface of the PZT-D freely suspended in air are shown in Figure 2e,f for the 2 dominant resonance modes (f_r (220 kHz), and f_t (1,08)). The radial mode (Figure 2e) is the first and fundamental mode of vibration, showing 1 displacement node and 1 displacement antinode. The thickness mode at 1 MHz is the third harmonic mode of vibration, presenting 2 nodes and 3 anti-nodes as demarcated by the nodal rings in Figure 2f. The displacement is in the order of 1–20 nanometers for a $10 V_{pp}$ pure sinusoidal signal at the driving frequency. Figure 2e shows higher displacement peaks at f_r , as compared to the value for a 2-mm thick PZT-D as shown in Figure 2c,d. This can be attributed to the energy being focused in a narrow frequency band for multiple cycles for a continuous pure sine as compared to application for a single cycle at each frequency step in the case of a sweep. The analytical modeling and Bessel fits for the radial components of the displacement at the two resonance modes are discussed in (Section S2, Supporting Information).

2.1.2. Impact of the Flexible Substrate on Mode Shapes and Peak Displacements

The addition of flexible substrates on piezoelectric transducers can not only provide mechanical stability but also result in

improved electromechanical response and flexibility. However, purely in terms of modal analysis, addition of a substrate to a piezoelectric transducer can significantly alter the vibrational behavior (natural frequency and modes) of the device due to a shift of the neutral axis. Therefore, the substrate material and geometry were selected such that the natural frequencies and vibrational modes on the ultrasound modes were not altered significantly. PDMS serves as an excellent material for microfluidic devices. Properties such as resistance to biodegradation, chemical stability, biocompatibility, and physiological indifference make it a good substrate material for ultrasound-based drug delivery devices. Moreover, for this particular application, the substrate acts as a good base for adhesive to maintain contact with the skin, and structurally patterned 1 mm-deep cavities around the PZT-D elements act as an active drug reservoir during sonophoresis. The PDMS substrate has a thickness of 1 mm which shifts the radial and thickness mode resonance frequencies to 225 and 996 kHz respectively. The low thickness of the substrate is selected to minimize the shift of resonant frequencies compared to the initial radial (220 kHz) and thickness (1 MHz) modes of the substrate-free transducer. The addition of PDMS substrate ultimately results in an insignificant shift in the neutral axis while still providing mechanical stability and improved electromechanical response.

Figure 3 illustrates the impact of the PDMS substrate on the operational modes of the transducer. In the absence of the PDMS substrate, the PZT-D experiences low deformation due to the high stress and a bulk of the residual energy is dissipated. The addition of the PDMS layer allows for the dissipated energy to be translated to the substrate, resulting in significantly higher displacement in the PDMS layer. The effect of the energy translation can be seen in the log scale Figure 3c,d, where the bottom of the transducer is shown. The PDMS layer experiences significantly higher displacement than the piezo layer as expected. It must be noted that, intentionally, the deformation of the piezo with and without the PDMS are similar due to vibrational behavior of the transducer being unchanged even in the presence of a thin substrate.

2.2. Acoustic Pressure Distribution of the PZT-D in Water Tank

It is desirable to characterize the acoustic pressure fields close to the PZT-D to estimate the spatial likelihood of cavitation. However, measuring the pressure experimentally using a hydrophone is extremely sensitive to reflections in the measurement setup and coupling from the electromagnetic field close to the transducer. These artifacts appear as jagged kinks in the experimentally measured pressure curves shown in Figure 4d. Here we aim to simulate various configurations of the measurement setup to determine the optimal boundary conditions in a water-tank to guarantee quality capture of hydrophone data. We then measure the pressure experimentally in this configuration and compare the data with a simulated pressure-frequency sweep at a fixed distance of 1, 2, and 3 cm from the transducer surface. This verified simulation model is then used to predict near-field pressure in the PDMS cavities for the final patch design, discussed subsequently in Section 2.3.

In order to solve the wave equation in the fluid media surrounding the piezo transducer, the physics interface of “Pressure

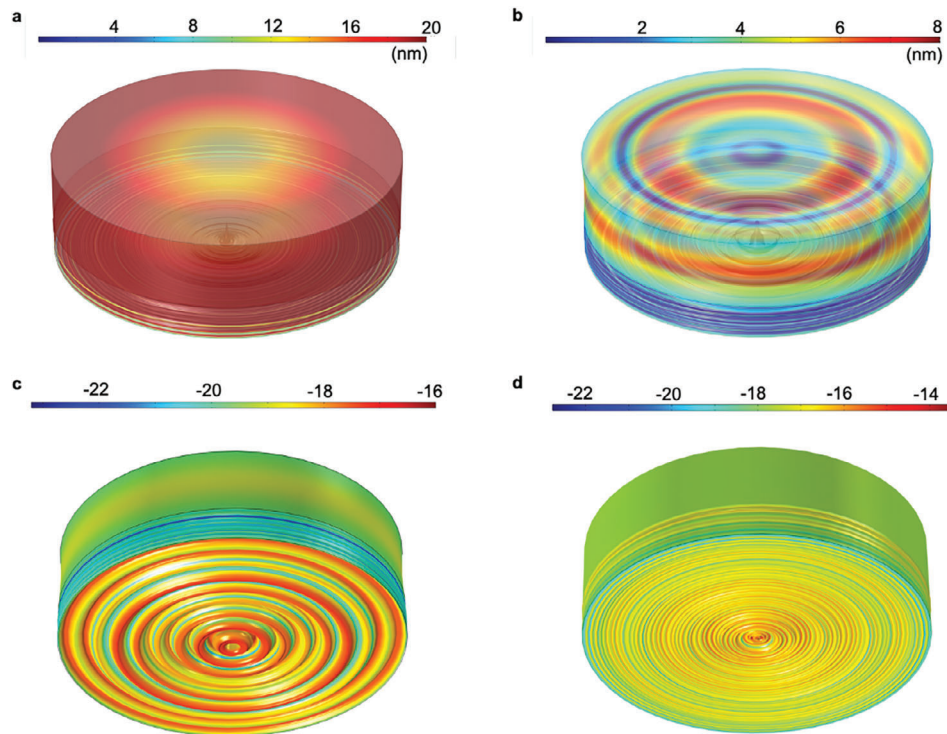


Figure 3. Impact of PDMS substrate on mode shape and displacement of the PZT-D. PZT-D with 1 mm-thick PDMS substrate at the bottom, showing peak displacements (capped at 20 and 8 nm respectively) across the top surface of the PZT-D for a) radial (220 kHz) and b) thickness mode (1 MHz). The PZT-D is driven at $10 V_{pp}$. Log of displacement in PDMS substrate at the bottom of the PZT-D for c) radial and d) thickness mode.

Acoustics, Frequency Domain” interface module is added to the previous COMSOL Multiphysics FEA model developed for the numerical simulations. The physical field of acoustic pressure is explored in the frequency domain and contains the partial differential equations (PDEs) known as the Helmholtz equations described as the following wave equation:

$$\nabla \cdot \frac{-\nabla p(x, y)}{\rho} - \frac{\omega^2 p(x, y)}{c^2 \rho} = 0 \quad (1)$$

where ω , c , and ρ represent the frequency of wave propagation, speed of the wave in the water, and density of water, respectively, and $p(x, y, t)$ represents the scattered acoustic pressure field in terms of the Cartesian coordinate for the spatial domain (x and y) and time (t). The model simply assumes that the acoustic source is made up of numerous point sources, with each point source contributing to the overall pressure field at that location, and it is used to produce the pressure field at frequencies matching the vibrational modes.

The lumped parameter electromechanical acoustic model can be expressed as:^[31] $[K]\{u\} - \omega^2[M]\{u\} + \omega jZ(p, \omega)\{u\} = \{0\}$ where $[K]$, $[M]$ are matrices of stiffness and mass, $\{u\}$ is the displacement, ω is the frequency, $Z(p, \omega)$ is the complex acoustic coupling dependent on the acoustic pressure, p and frequency, ω .

Boundary conditions are critical constraints in COMSOL Multiphysics simulations. They are defined based on the pressure acoustics module considering the sound hard boundary wall

which assumes that the normal component of the acceleration, velocity, and the normal derivative of the pressure are zero at the boundary; $\frac{\partial p}{\partial n} = 0$. The spherical wave radiation is a radiating field source located at $z_0 = 0$. The water medium has a 10 cm x 10 cm surface area. We have tested three different boundary conditions which are shown in Figure 4a–c. The true absolute pressure measurements correspond to Figure 4a, with plane-wave propagation conditions assigned to both the top (air-water surface) and side walls of the tank. This assumes that the water medium continues infinitely in both directions presenting no reflections, and the pressure field is representative of the true values. The amplitude of the pressure decreases gradually along z toward the air-water interface (Figure 4a, right). Next, in Figure 4b, we simulate the case of a water-air interface at top surface, and a reflective water-glass-air interface at the side walls. This creates a standing-wave pattern within the tank (Figure 4b, left), and presents many time-varying artifacts in the pressure amplitude across the tank as seen in the plot given alongside which results in an over- or under-estimation of the true pressure at any given location. Next, we simulate a case with an open water tank (air-water interface at the top) and acoustic dampeners (AptFlex F28, Precision Acoustics) on the side walls to minimize reflections by assigning plane-wave propagation at the sides of the model tank (Figure 4c). This case shows remarkable similarity with the ideal case in both the wave pattern and the rate of decrease of the pressure amplitude. This configuration is also feasible to set up in practicality and is chosen to make the far-field pressure measurements shown in Figure 4d.

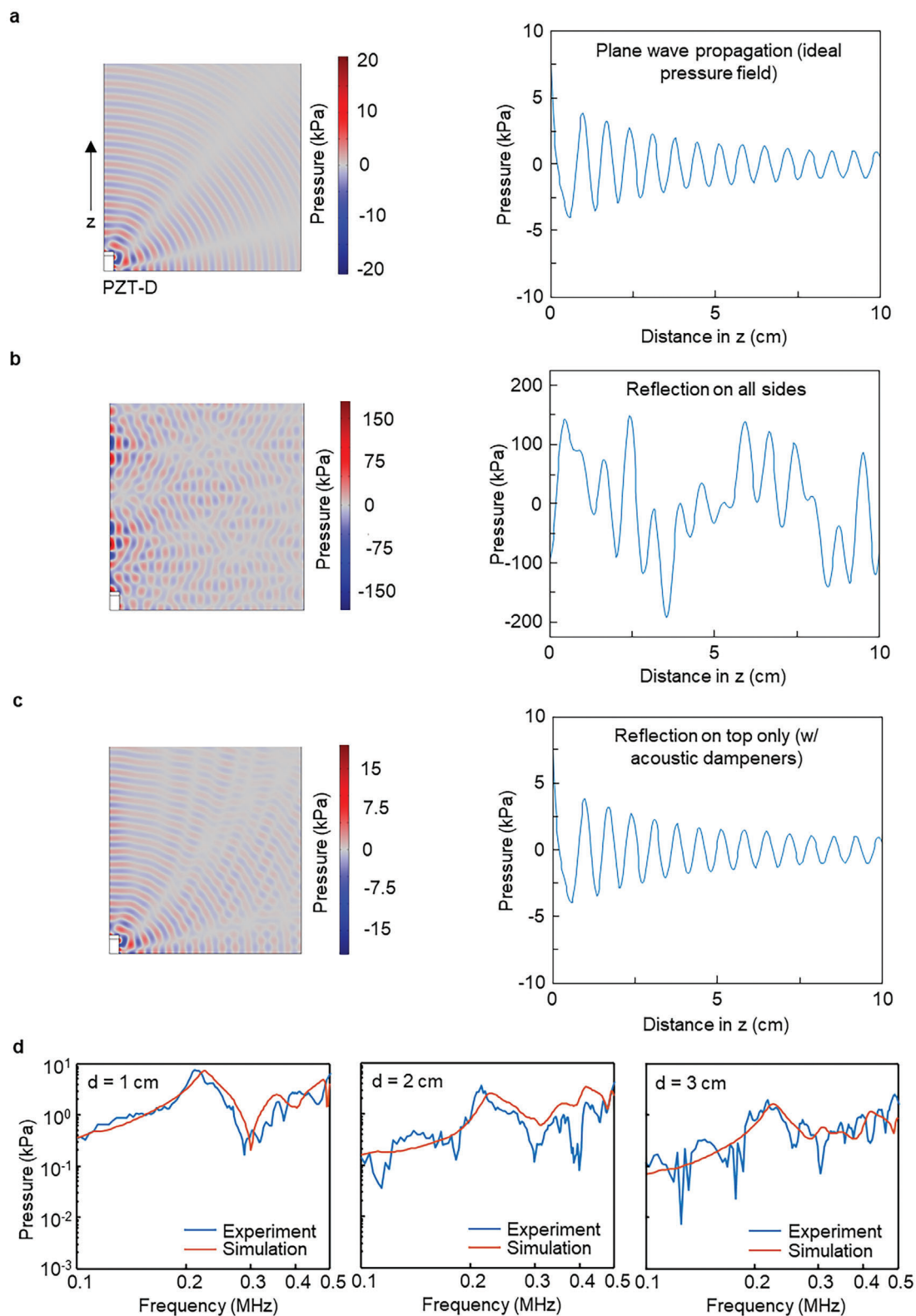


Figure 4. Impact of water-tank dimensions, reflections, and need for acoustic dampers. 2D axis-symmetric acoustic pressure distribution in water (left side) and along the z-axis through the center of the PZT-D (right side) for a) ideal boundary conditions with no reflections, b) reflective water-air boundary on top and water-glass-air side-walls and c) reflective water-air boundary on top, and acoustically damped side-walls. d) Experimentally measured (blue) and simulated (red) frequency-sweep plots (100–500 kHz) for pressure at distances of 1, 2, and 3 cm along the z-axis. Note that all pressures are in kPa, and the y-axis propagates through the 3 plots in Figure 4d.

The pressure results are evaluated by comparing the experimental and simulated pressure results across different distances from the surface of the device. In this study, we are interested in the investigation of the resonant frequency in the lower frequency range of 220 kHz, since the cavitation thresholds are lower at this frequency range. To evaluate the acoustic pressure profile, the PZT-D was immersed into a tank ($49.5 \times 25.0 \times 29.0 \text{ cm}^3$) filled with deionized (DI) water with a hydrophone (HGL-0200, Onda Corp.) pointed directly along the central axis of the device. A burst mode sinusoid was used to determine the distance between the hydrophone and device and a frequency-swept sinusoidal signal (100–500 kHz) was used as the excitation signal. A function generator (Model 3390 Arbitrary Waveform Generator, Keithley) was used to achieve the desired voltage output at $10 V_{pp}$. The generated ultrasound pressure was then characterized with the hydrophone at different distances away from the PZT-D (1, 2, and 3 cm) using a spectrum analyzer (NanoVNA-H, Seesii). The experimental results were filtered using a low pass filter in MATLAB.

Figure 4d shows the pressure results at the distance of 1, 2, and 3 cm away from the surface of the device in water. The results show that the resonant frequency is independent of the location of measurement in the water tank as the distance increases from the surface of the device: however, the pressure amplitude and the fluctuations of the experimental results are affected. The pressure at the resonant frequencies decreases from 9 to 3 kPa and 2 kPa as the hydrophone is moved from 1 to 2 cm and 3 cm away from the surface of the device for a driving voltage of $10 V_{pp}$. At distances closer than 1 cm from the surface of the piezoelectric disk transducer, it was not possible to make near-field experimental measurements due to electromagnetic coupling into the hydrophone by the piezo driver.

Despite the simplicity of the FEA model, the simulation results match the results of the experiments that were conducted in terms of efficient description of the resonant frequency and amplitude of pressure. The fluctuations could be caused by alignment issues, noise, and the distortions from the hydrophone. Nonetheless, the FEA model remains a useful tool for initial approximation of acoustic pressure.

2.3. Modeling of the Multi-Element Patch for In Vitro Trials

Up to this point, the scope of modeling of the conformable ultrasound face patch was limited to a single element. However, achieving drug delivery across an entire region such as the cheek or forehead demands a conformable patch with 2D arrangement of elements. The effect of skin, the encapsulating polymer, and any interaction or coupling between the PZT-D elements is subsequently investigated.

Figure 5a–c illustrates the 3D view and 2D cross-sectional view of the array elements of the ultrasound patch used in our FEM simulations for modeling the in vitro trials when the device has adhered to facial skin. The geometry is composed of 4 PZT-Ds arranged in a 2×2 configuration and encapsulated in a soft PDMS substrate with a total thickness of 4 mm. Circular cavities of 6 mm radius and 3 mm depth are patterned concentrically around the PZT-D elements in the PDMS substrate. The cavity is filled with the drug solution (3% w/w so-

lution of niacinamide dissolved in a phosphate-buffered saline), and it acts as a drug reservoir while providing a controlled space for cavitation action of bubbles against the skin surface. For all practical purposes, the drug solution can be modeled as water as it presents comparable density (1.073 g mL^{-1}) and viscosity (1.00 ± 0.05). The PZT-Ds are driven in parallel with a sinusoidal voltage of $50 V_{pp}$. Further details on the modeling and material properties can be found in Section S1 (Supporting Information).

Several features are of interest within the 2D array of the transducers. First, to study the impact of PZT-D spacing, a simplified configuration is considered wherein the PZT-Ds are arranged on a flat PDMS substrate without the patterned cavities (Figure 5a). A 2 mm layer of skin is applied at a separation distance of 1 mm from the top surface of the PZT-Ds. The cross-section through a set of 2 PZT-Ds is taken to generate the pressure maps (Figure 5b). 3 PZT-D separation distances are considered – 10, 4, and 2 mm as shown in Figure 5d, and examined across plane CSA1 as shown in Figure 5b. Peak pressures of $\approx 180 \text{ kPa}$ are generated within the fluid medium in all 3 configurations, showing that it is possible to generate pressures larger than the cavitation threshold ($\approx 100 \text{ kPa}$) in all three cases. The main lobes of peak pressures are contained within a small region directly above the center of each PZT-D at all separation distances. As the distance between two adjacent PZT-Ds in an array is reduced, the side lobes of pressure from each PZT-D element generate patterns of constructive interference, creating spikes in pressure and increasing the total area within the fluid conducive to the nucleation of cavitation. As a quantitative indicator of this effect, the peak pressure is plotted at a point P1 directly between 2 PZT-Ds (Figure 5c,f). The pressure at P1 drops to 50% of its peak value at around 3 mm separation. This provides a good directive to design the PZT-Ds as close to each other as possible without compromising the mechanical stability of the patch. The variation in absolute pressure along the z-direction above the center of the PZT-D in an array is demonstrated in Figure 5e. The pressure drops off steeply below the cavitation threshold when the distance in z is $>1.5 \text{ mm}$, and it is thus desirable to position the skin within this distance. The final configuration of the patch with 10 mm PZT-D spacing and structural PDMS cavities placed against the skin is shown in Figure 5g. The pressure in both the fluid coupling medium and the skin is plotted in a continuum. Since the acoustic impedances of the two are comparable, there is minimal distortion of the pressure field at the fluid-skin interface. The side lobes of pressure are suppressed due to the structural PDMS columns between the PZT-D elements. In future iterations of the design, it is desirable to reduce the size and thickness of the PDMS columns to facilitate constructive interferences of the side lobe pressures and increase the likelihood of cavitation.

The results demonstrate that for in vivo trials, the piezoelectric transducer can be encapsulated in a soft PDMS substrate with little sacrifice to the pressure amplitude in the coupling medium. Further, it is shown that the distance between the piezoelectric elements can have a certain degree of influence on the acoustic pressure distribution, but undamped pressure zones in excess of $\approx 140 \text{ kPa}$ are formed within the medium in all configurations of the patch. Ex vivo studies of the device demonstrate highly effective sonophoresis action of the device, providing a 26.2-fold

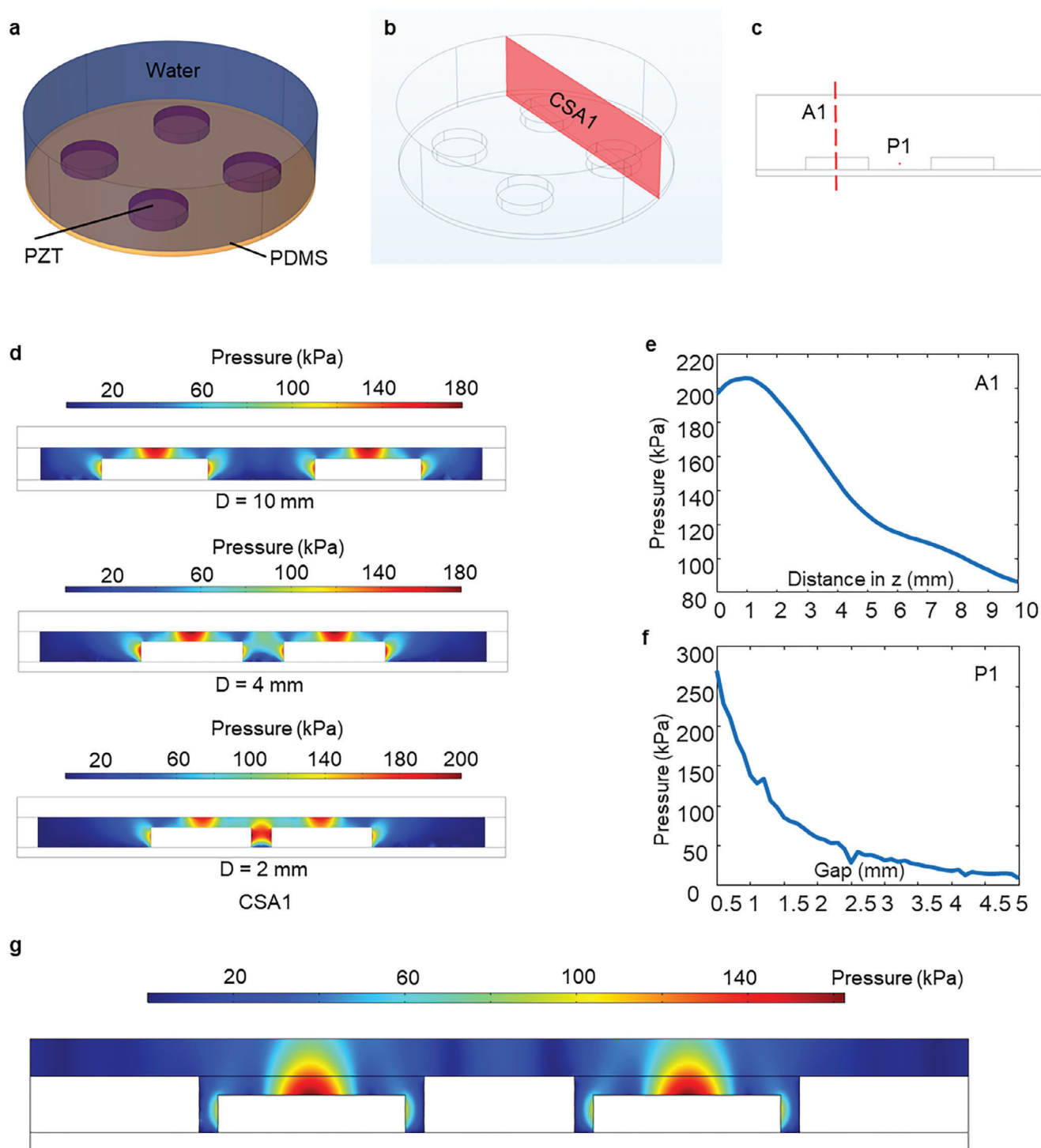


Figure 5. Modeling for ultrasound patch for in-vivo trial. a) Simplified arrangement of 2×2 array of PZT-D elements on a 1-mm thick PDMS substrate. b) Cross-section considered across two PZT-D elements for the pressure maps. c) Axis A1 through the center of the PZT-D element, and point P1 between 2 PZT-D elements, positioned 1 mm from the top of the PDMS substrate. d) Pressure distribution in fluid coupling medium for CSA1 for different PZT-D separation distances (10, 4, and 2 mm, top to bottom). e) Pressure profiles along axis A1, starting at the surface of the PZT-D element. f) Pressure profile at point P1 for different separation gaps between the PZT-D elements. g) Pressure distribution for final patch design with 10-mm PZT-D separation and structurally patterned PDMS cavities. All pressures correspond to a driving voltage of $50 V_{pp}$.

enhancement in the delivery of niacinamide through full thickness porcine skin.^[32]

The scope of this study describes the interactions of acoustic pressure fields created by identical PZT-D elements driven at a single resonance frequency. The effect of increasing the number of PZT-Ds in 2D multi-element configurations is considered stepwise in Figures S3.1 and S3.2 (Supporting Information). For dual-frequency sonophoresis or multi-element patches with different PZT-D elements, it is important to characterize the individual pressure fields and the pairwise interaction of the elements before running a multi-element study. For example, a low-frequency PZT-D can be used to nucleate bubbles which are acted upon by high-frequency pressure regimes to grow and stabilize the bubbles. The phase of the individual pressure fields and their spatial congruence and overlap must be taken into account to achieve the desired effect by the PZT-D pair.

3. Conclusion

Wearable and conformable smart-sensing and actuation platforms for various applications,^[27,33,34] are becoming increasingly relevant, and this paper presents a framework for analyzing and modeling a conformable piezoelectric transducer patch for enhancing transdermal drug delivery through acoustic cavitation. First, the geometry-dependent electromechanical behavior of the piezoelectric transducer is characterized, and the resulting mode shapes and components of displacement are resolved for the two dominant modes of resonance. The impact of polymeric encapsulation on the resonant frequency and peak displacements of the PZT-D elements are studied to determine feasibility of integrating rigid device components into conformable platforms. The design of these conformable acoustic interfaces between device and skin is of growing interest in the emerging field of wearable ultrasound electronics.^[35] Next, simulations are carried out to determine optimal conditions in a water tank for capturing acoustic pressure data using a hydrophone. Practical measurements of acoustic pressure in fluid are often confounded by reflections in the measurement tank, leading to variable outcomes in the absolute pressure measured at various locations. A systematic analysis is carried out to determine the optimal configuration for experimental measurements by simulating various boundary conditions. A 20 cm × 20 cm water tank with acoustic absorbers on the side and an open surface on the top is chosen, and the experimentally measured pressure values in the far-field are shown to be in excellent agreement with the simulated values, validating the FEM model. The near-field pressure close to the PZT-D surface (< 1 cm) is then characterized using simulations for 2D arrays of PZT-D elements in various configurations on soft substrates. This pipeline of FEM models can be used for simulation-based rapid iteration and optimization of designs for ultrasound piezoelectric actuators on conformable platforms for various applications. In the future, experimental measurements of the acoustic pressure taken in an *ex vivo* setup with porcine skin^[32] would be a valuable addition to this characterization flow. Further, the application of dual-frequency ultrasound is also recommended due to its superior enhancement effects observed *in vivo*,^[36,37] The effects of using these PZT-Ds in different resonance modes on the acoustic pressure interactions between the PZT-D elements and the resulting cavitation regime can be systematically mod-

eled as per the approach shown in Section 2.3 and Figures S3.1 and S3.2 (Supporting Information). A rigorous understanding of these soft ultrasound platforms on tissue will open up avenues for the development of sophisticated conjugate systems of topical ultrasound acting upon implantable^[38] or subcutaneous^[39] sono-responsive mediums^[40] for safe, non-invasive, and enhanced effect *in vivo*.

Supporting Information

Supporting Information is available from the Wiley Online Library or from the author.

Acknowledgements

N.A. and A.S. contributed equally to this work. C.D. thanks H. Emre Dagdeviren for fruitful discussions throughout this project. A.S. thanks Rajeev Shah for the valuable discussions on structures and materials. This work was supported by the National Science Foundation CAREER: Conformable Piezoelectrics for Soft Tissue Imaging (grant no. 2044688), 3 M Non-Tenured Faculty Award, and MIT Media Lab Consortium funding. A.S. was supported by the K. Lisa Yang Bionics Center Graduate Fellowship Program. This work was performed primarily at the Media Lab, Massachusetts Institute of Technology (MIT), USA. This project was also supported by the National Science Foundation Collaborative Research: Controlling Flow Separation via Traveling Wave Actuators (grant no. s1905252).

Conflict of Interest

The authors declare no conflict of interest.

Author Contributions

C.D. and A.K. conceived the overall research goals and aims. N.A., A.K.B., and A.K. designed the models. N.A., A.S., and A.K.B. conducted the FEM and contributed to device design and results interpretation. C.Y. and A.S. conducted the water-tank experiments, performed data analysis, and organized the results. All authors contributed to the manuscript writing.

Data Availability Statement

The data that support the findings of this study are available from the corresponding author upon reasonable request.

Keywords

acoustic cavitation, conformable devices, FEM, piezoelectric materials

Received: November 13, 2023

Revised: January 25, 2024

Published online:

- [1] G. M. Shingade, *J. Drug Delivery Ther.* **2012**, *2*, 66.
- [2] N. V. D., N. Shrestha, J. Sharma, *Int. J. Res. Pharm. Sci.* **2012**, *3*, 234.
- [3] S. Dharadhar, A. Majumdar, S. Dhoble, V. Patravale, *Drug Dev. Ind. Pharm.* **2019**, *45*, 188.

- [4] B. W. Barry, *Eur. J. Pharm. Sci.* **2001**, *14*, 101.
- [5] M. A. Luzuriaga, D. R. Berry, J. C. Reagan, R. A. Smaldone, J. J. Gassensmith, *Lab Chip* **2018**, *18*, 1223.
- [6] Y. N. Kalia, A. Naik, J. Garrison, R. H. Guy, *Adv. Drug Delivery Rev.* **2004**, *56*, 619.
- [7] A.-R. Denet, R. Vanbever, V. Pr eat, *Adv. Drug Delivery Rev.* **2004**, *56*, 659.
- [8] R. Rao, S. Nanda, *J. Pharm. Pharmacol.* **2010**, *61*, 689.
- [9] E. C. Jung, H. Zhu, Y. Zou, A. Elmahdy, Y. Cao, X. Hui, H. I. Maibach, *Int. J. Cosmet. Sci.* **2016**, *38*, 646.
- [10] J. Park, H. Lee, G.-S. Lim, N. Kim, D. Kim, Y.-C. Kim, *AAPS Pharm-SciTech* **2019**, *20*, 96.
- [11] M. R. Prausnitz, R. Langer, *Nat. Biotechnol.* **2008**, *26*, 1261.
- [12] M. R. Prausnitz, S. Mitragotri, R. Langer, *Nat. Rev. Drug Discovery* **2004**, *3*, 115.
- [13] J. Robertson, S. Becker, *Ultrasound Med. Biol.* **2018**, *44*, 1100.
- [14] F. Iliopoulos, B. C. Sil, A. S. M. Monjur Al Hossain, D. J. Moore, R. A. Lucas, M. E. Lane, *Int. J. Pharm.* **2020**, *579*, 119137.
- [15] J. Rooze, E. V. Rebrov, J. C. Schouten, J. T. F. Keurentjes, *Ultrason. Sonochem.* **2013**, *20*, 1.
- [16] T. Terahara, S. Mitragotri, J. Kost, R. Langer, *Int. J. Pharm.* **2002**, *235*, 35.
- [17] R. Martinez, A. Vera, L. Leija, presented in *2014 IEEE Int. Instrumentation and Measurement Technology Conference (I2MTC) Proc*, IEEE, Montevideo, Uruguay, May, **2014**, pp 299–303.
- [18] N. Guo, P. Cawley, D. Hitchings, *J. Sound Vib.* **1992**, *159*, 115.
- [19] A. Bhargava, S. Shahab, *J. Intell. Mater. Syst. Struct.* **2021**, *32*, 1215.
- [20] N. V. Thinh, *Int. J. Eng. Res.* **2019**, *8*, 6.
- [21] Z. Wei, L. K. Weavers, *Ultrason. Sonochem.* **2016**, *31*, 490.
- [22] W. Du, L. Zhang, E. Suh, D. Lin, C. Marcus, L. Ozkan, A. Ahuja, S. Fernandez, I. I. Shuvo, D. Sadat, W. Liu, F. Li, A. P. Chandrakasan, T. Ozmen, C. Dagdeviren, *Sci. Adv.* **2023**, *9*, eadh5325.
- [23] L. Zhang, C. Marcus, D. Lin, D. Mejorado, S. Joseph Schoen, T. T. Pierce, V. Kumar, S. V. Fernandez, D. Hunt, Q. Li, I. Iftekhar Shuvo, D. Sadat, W. Du, H. Edenbaum, L. Jin, W. Liu, Y. C. Eldar, F. Li, A. P. Chandrakasan, A. E. Samir, C. Dagdeviren, *Nat. Electron.* **2023**, *7*, 91.
- [24] S. V. Fernandez, D. Sadat, F. Tasnim, D. Acosta, L. Schwendeman, S. Shahsavari, C. Dagdeviren, *Foresight* **2022**, *24*, 75.
- [25] F. Tasnim, A. Sadraei, B. Datta, M. Khan, K. Yun Choi, A. Sahasrabudhe, T. A. V. G alvez, I. Wicaksono, O. Rosello, C. Nunez-Lopez, C. Dagdeviren, *Foresight* **2018**, *20*, 589.
- [26] C. Dagdeviren, Y. Shi, P. Joe, R. Chaffari, G. Balooch, K. Usgaonkar, O. Gur, P. L. Tran, J. R. Crosby, M. Meyer, Y. Su, R. C. Webb, A. S. Tedesco, M. J. Slepian, Y. Huang, J. A. Rogers, *Nat. Mater.* **2015**, *14*, 728.
- [27] T. Sun, F. Tasnim, R. T. McIntosh, N. Amiri, D. Solav, M. T. Anbarani, D. Sadat, L. Zhang, Y. Gu, M. A. Karami, C. Dagdeviren, *Nat. Biomed. Eng.* **2020**, *4*, 954.
- [28] J. Yuan, C. Dagdeviren, Y. Shi, Y. Ma, X. Feng, J. A. Rogers, Y. Huang, *Proc. R. Soc. A* **2016**, *472*, 20160225.
- [29] H. Zhao, C. Dagdeviren, G. Liu, P. Cao, J. Wang, B. Sha, G. Wang, J. Cui, Y. Su, *Extreme Mech. Lett.* **2022**, *55*, 101801.
- [30] C. Piao, J. O. Kim, *J. Mech. Sci. Technol.* **2016**, *30*, 5351.
- [31] A. Hajati, D. Latev, D. Gardner, A. Hajati, D. Imai, M. Torrey, M. Schoeppler, *Appl. Phys. Lett.* **2012**, *101*, 253101.
- [32] C.-C. Yu, A. Shah, N. Amiri, C. Marcus, O. Goni Nayeem, A. K. Bhayadia, A. Karami, C. Dagdeviren, *Adv. Mater.* **2023**, *35*, 2300066.
- [33] J.-H. Kim, C. Marcus, R. Ono, D. Sadat, A. Mirzazadeh, M. Jens, S. Fernandez, S. Zheng, T. Durak, C. Dagdeviren, *Nat. Electron.* **2022**, *5*, 794.
- [34] C. Dagdeviren, Y. Su, P. Joe, R. Yona, Y. Liu, Y.-S. Kim, Y. Huang, A. R. Damadoran, J. Xia, L. W. Martin, Y. Huang, J. A. Rogers, *Nat. Commun.* **2014**, *5*, 4496.
- [35] L. Zhang, W. Du, J. Kim, C. Yu, C. Dagdeviren, *Adv. Mater.* **2023**, *2307664*.
- [36] C. M. Schoellhammer, S. Srinivasan, R. Barman, S. H. Mo, B. E. Polat, R. Langer, D. Blankschtein, *J. Control Release* **2015**, *202*, 93.
- [37] C. M. Schoellhammer, B. E. Polat, J. Mendenhall, R. Maa, B. Jones, D. P. Hart, R. Langer, D. Blankschtein, *J. Control Release* **2012**, *163*, 154.
- [38] D. Huang, L. Cai, N. Li, Y. Zhao, *Smart Med.* **2023**, *2*, e20230003.
- [39] Q. Zeng, G. Li, W. Chen, *Adv. Drug Delivery Rev.* **2023**, *203*, 115133.
- [40] D. Huang, J. Wang, J. Che, B. Wen, W. Kong, *Biomed. Technol.* **2023**, *1*, 1.